applied sciences

MDPI

Article

Investigation of Strain of Steel Reinforcement of Modular Flexural Member at Discontinuity Interface

Jongho Park [1], Hae-Kyun Lee [1], Sun-Kyu Park [1], Jinwoong Choi [2] and Sungnam Hong [3,*]

[1] Department of Civil, Architectural and Environmental System Engineering, Sungkyunkwan University, Suwon 16419, Gyeonggi-do, Korea; rhapsode@skku.edu (J.P.); haekyun@msn.com (H.-K.L.); skpark@skku.edu (S.-K.P.)

[2] Structure Research Division, Korea Expressway Corporation Research Institute, Hwaseong 18489, Gyeonggi-do, Korea; jchoi@ex.co.kr

[3] Department of Ocean Civil Engineering, Gyeongsang National University, Tongyeong 53064, Gyeongsangnam-do, Korea

* Correspondence: snhong@gnu.ac.kr; Tel.: +82-055-772-9121

Received: 15 October 2019; Accepted: 11 November 2019; Published: 15 November 2019

Abstract: The modular structure has a discontinuity owing to the joint between the modules; thus, structural behavior verification is required. In this study, the tensile behavior of a steel reinforcement at the discontinuity interface was evaluated in the joint of a modular flexural member. The modular specimen was fabricated with a 400 mm joint, and an integral specimen was fabricated with the same specifications as the modular specimen, without a joint. The largest crack width of the integral specimen was measured at the center of the beam, and that of the modular specimen was measured at the discontinuity interface. The maximum crack width of the modular specimen was greater than that of the integral specimen. The strain of the steel reinforcement was estimated using the measured crack width and six formulas for evaluating the crack width. The estimated strain of the modular specimen was higher than that of the integral specimen, and the deformation of the steel reinforcement at the discontinuity interface was accelerated with the increasing load. Therefore, the tensile load was concentrated at the discontinuity interface in the modular specimen, and the steel reinforcement at the discontinuity interface was likely to yield earlier than the integral specimen.

Keywords: prefabricated structure; joint discontinuity; tensile reinforcement; strain estimation; crack width

1. Introduction

Infrastructures suffer performance degradation owing to accidents and natural disasters, or they fail to satisfy the required durability and performance criteria because of aging. This affects the safety of structures; thus, the performance of infrastructures needs to be improved. Accordingly, various maintenance methods for structures have been proposed [1–3], and repair and strengthening methods, such as fiber-reinforced polymer (FRP) and textiles, have been proposed and applied [4–7].

Construction of new structures is needed because of the problem of the durability and safety decreasing over time for old structures despite maintenance, repair, and strengthening. However, ordinary construction methods are unsatisfactory because they require a long construction period, resulting in problems such as environmental impact and restriction of traffic, which lead to overhead costs. Research on prefabricated structures adopting the modular concept has been performed because they can ensure a certain quality owing to the shorter construction period, minimal environmental impact, cost reduction, and partial replacement of damaged components [8–11]. However, because prefabricated structures have discontinuities owing to the joints between modules, the structural performance of members with joints should be verified [12–14].

Buyukozturk et al. [15], Issa et al. [16], Kim et al. [17], and Lee et al. [18] verified the structural performance according to the shape of the joint and conducted analytical studies. Shah et al. [19] and Zhu et al. [20] proposed a new connection method. However, the experiments in these studies were performed to verify the structural performance according to the joint shape and connection method between precast modules and involved various variables and site conditions; thus, there were limitations for the general prediction of the joint behavior.

POSCO [9] conducted design and structural performance verification studies on girder and slab-type precast modular bridges. On the basis of their results, various studies were conducted. The behavior of a modular bridge was analyzed according to the cyclic load, and a joint design procedure was proposed [12]. Lap splices were redesigned from ultimate strength design to limit state design in order to improve the stability and moment strength of the joint [21]. The difference in the crack progress was reported, and the characteristics of the joint in the modular member on the cyclic load were analyzed in terms of the moment of inertia [22]. Additionally, a calculation method for the deflection of the modular member considering the strength of the precast module and the joint was proposed [23], and the mean steel reinforcement strain of the modular member was evaluated using the compressive strength of the concrete and the ratio of reinforcement [24]. However, these studies compared the load and deflection of the modular member with those of the integral member and evaluated the performance without analyzing the joint behavior. Thus, the theoretical approach to characterizing the joint behavior was insufficient. Hence, the objective of the present study was to evaluate the behavior of modular members quantitatively through estimation of the steel reinforcement tensile strain using crack width [25].

2. Experimental Program

2.1. Specimen

A slab-type specimen with a length of 3400 mm, a width of 1000 mm, and a height of 220 mm was fabricated. The modular specimen was fabricated by connecting two precast modules with a compressive strength of 50 MPa. The joint was fabricated using a H16 steel reinforcement bar with a tensile strength of 400 MPa and lap splices 200 mm long. To minimize the connecting width and improve the durability of the joints, ultra-high-strength concrete with a strength of 120 MPa was used. For the other reinforcements, H13, H10 with a tensile strength of 400 MPa was used. An integral specimen with the same size as the modular specimen was fabricated using 50 MPa concrete. The specifications of the modular specimen are shown in Figure 1. The mix proportions of the 50 and 120 MPa concrete are presented in Table 1.

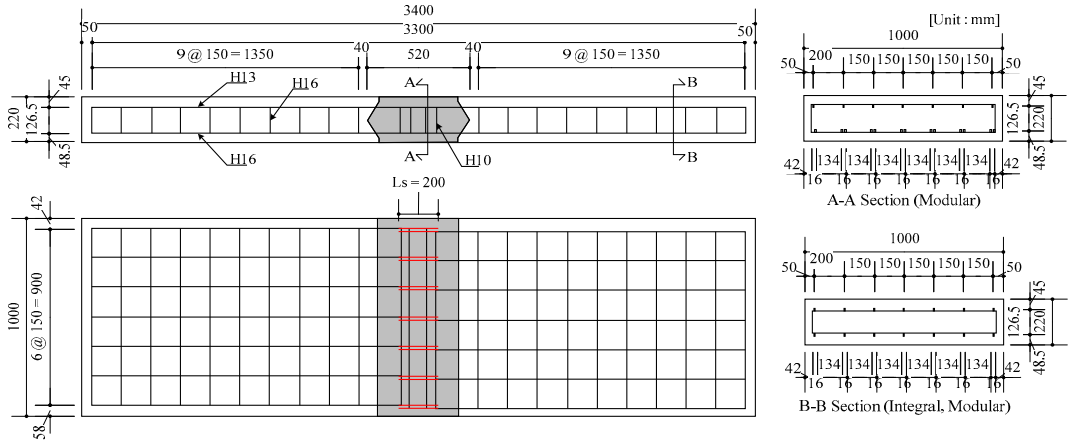

Figure 1. Specifications of the modular specimen.

Table 1. Mix proportions of 50 and 120 MPa concrete.

Strength	W/B (%)	S/a (%)	(kg/m^3)											Fiber (Vol%)	AD (B*%)
			W	OPC	BS	SF	Ω	EA	RS	FA	S	G13	G25		
50	31.9	50	185	290	174	-	-	-	-	116	738		749	1.0	0.80
120	15.2	37.5	139	611	204	102	102	32	21	-	458	755		0.2	1.7

Where, W/B is the water–binder ratio, S/a is the sand–aggregate ratio, W is the water, OPC is the ordinary Portland cement, BS is the blast furnace slag, SF is the silica fume, Ω is the omega 2000 (ready-made by Hanil Cement Co., Ltd., Seoul, Korea), EA is the expansion agent, RS is the shrinkage-reducing agent, FA is the fly ash, S is the sand, G13 is the gravel (diameter = 13 mm), G25 is the gravel (diameter = 25 mm), Fiber is the polyamide fiber (diameter = 0.5 mm, tensile strength = 688.1 MPa), and AD is the liquid-type high early strength agent.

2.2. Test Setup

An experiment was performed using a universal testing machine. As shown in Figure 2, the four-point loading method was employed to introduce the maximum moment and pure flexural behavior at the joint part of the modular specimen. The span was 3000 mm, and the loading positions were 500 mm to the left and right of the center of the span. The load was applied at a rate of 0.05 mm/s until the specimen failed. To measure the tensile strain of the steel reinforcement for the two specimens, steel strain gauges were attached at points corresponding to 1/6, 2/6, 4/6, and 5/6 of the span of the specimen and denoted as S1, S2, S3, and S4, respectively. A crack gauge was installed at a position where the maximum crack width occurred; thus, the crack width was measured at the center of the integral specimen and the discontinuity interface of the modular specimen. Additionally, a linear variable differential transformer (LVDT) was installed at the center.

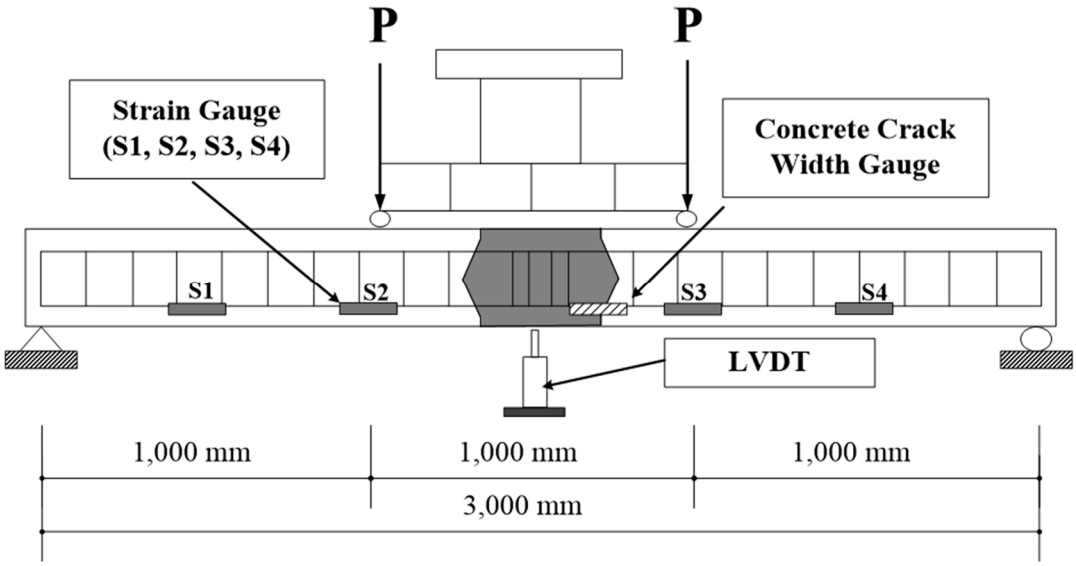

Figure 2. Test setup for the modular specimen.

2.3. Results and Discussion

2.3.1. Load and Deflection

The results for the load and deflection of the integral and modular specimens with the joint are presented Figure 3 and Table 2. For the modular specimen, the yield load was 96.1%, the ultimate load was 92.7%, and the deflection at specimen failure was 80.4% of that of the integral specimen. Choi et al. [12] reported the load-deflection behavior of two specimens to be very similar.

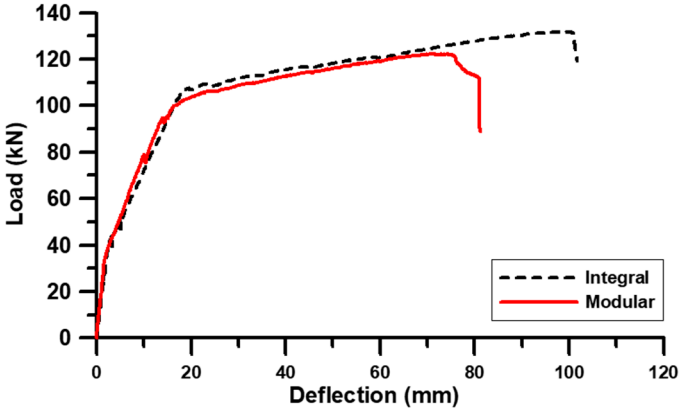

Figure 3. Load-deflection curve.

Table 2. Results of the static loading test for the integral and modular specimens.

Type	Yield Load (kN)	Ultimate Load (kN)	Deflection (mm)
Integral specimen	106.9	131.9	100.6
Modular specimen	102.7	122.3	80.9

2.3.2. Crack

Figure 4 shows the crack progression, which differed between the modular and integral specimens. The initial crack of the integral specimen exhibited a typical reinforced concrete flexural crack progression from the center to the support point. However, in the case of the modular specimen, the cracks initially occurred at the discontinuity interface and grew continuously, gradually reaching the loading point. Subsequently, a crack appeared on the tensile side of the concrete, at the joint.

(**a**) (**b**)

Figure 4. Crack progression: (**a**) integral specimen; (**b**) modular specimen.

The crack widths of the specimens are shown in Figure 5. The maximum crack width for the modular specimen was 1.21 mm, which was 327% larger than that for the integral specimen (0.37 mm) [26].

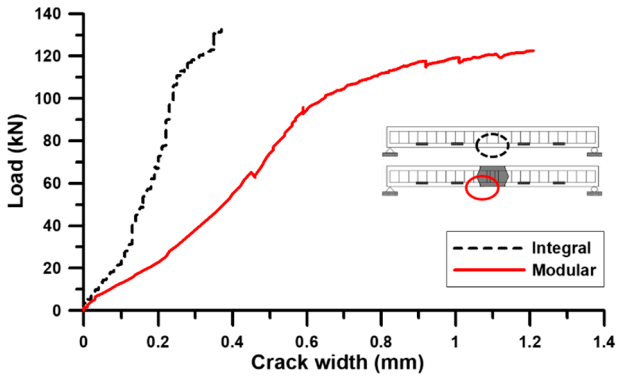

Figure 5. Crack width for the integral and modular specimens.

2.3.3. Steel Reinforcement Strain

Figure 6 and Table 3 show the results of load and reinforcement strain, ε_s. For both specimens, the strains at points S1 and S4 did not exhibit a significant change until the failure of the specimen. At loading positions S2 and S3, the steel reinforcement strains of the integral specimen were similar to that at S1 and S4 before the yield load was reached, and they increased rapidly from the yield load to the ultimate load. Additionally, for the modular specimen, the steel reinforcement strains at S2 and S3 were not significantly different from the strains at S1 and S4. The strains at S2 and S4 in the modular specimen exhibited similar behavior to those in the integral specimen until the yield load was reached, but there was no rapid increase in the strains after the yield load was reached [26]. Thus, the steel reinforcement strains of the integral specimen at loading positions S2 and S3 after the yield load was reached were greater than that of the modular specimen. Therefore, it is estimated that most of the steel reinforcement deformation of the modular specimen occurred at the discontinuity interface of the joint, considering that the crack at the discontinuity was 327% larger than the central crack of the integral specimen and that the initial failure pattern occurred at the joint.

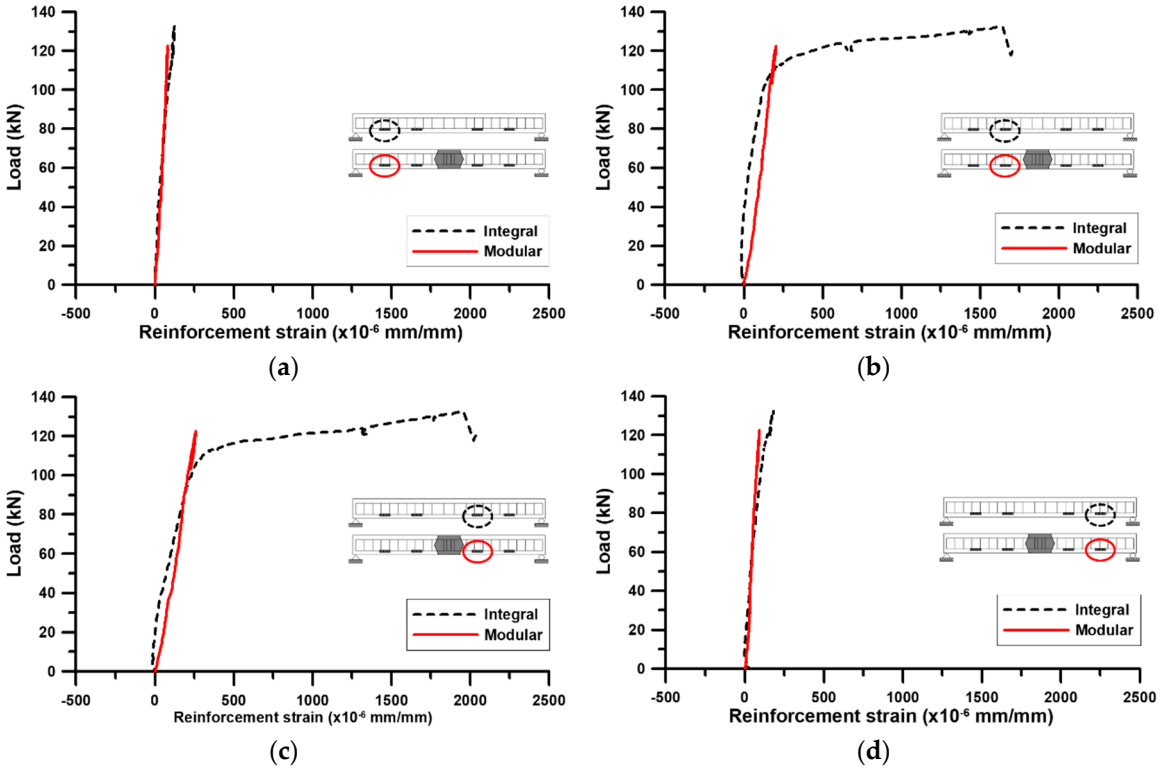

Figure 6. Reinforcement strain of the integral and modular specimens: (**a**) S1; (**b**) S2; (**c**) S3; (**d**) S4.

Table 3. Measured strain at location S1, S2, S3, and S4 of integral and modular specimen.

Location	Measured Strain of Integral Specimen ($\times 10^{-6}$ mm/mm)			Measured Strain of Modular Specimen ($\times 10^{-6}$ mm/mm)		
	At Service Load	At Yield Load	At Ultimate Load	At Service Load	At Yield Load	At Ultimate Load
S1 (500 mm)	39	91	124	45	65	82
S2 (1000 mm)	43	161	1642	111	150	204
S3 (2000 mm)	107	271	1956	144	186	259
S4 (2500 mm)	50	112	181	46	66	94

3. Estimation of Reinforcement Strain

3.1. Assumption and Crack Width

According to the results of the steel reinforcement strain and crack width measurement, the difference in behavior between the integral and modular specimens was identified. To analyze the steel reinforcement strain quantitatively according to the measured crack width, the following two assumptions were made.

1. There was no slippage of the steel reinforcement in the modular specimen, especially at the discontinuity interface.
2. The compressive strength of the joint concrete in the modular specimen was equal to that of the precast module.

Six crack width calculation formulas were employed to estimate the strain of the steel reinforcement according to the measured crack width, as shown in Table 4. Four formulas were based on the material model considering the tension stiffening effect in Eurocode2, and two formulas were based on the mean steel reinforcement strain for convenience of calculation in the Euro-Design Handbook [26–31]. The stress of steel reinforcement, f_{so}, was considered the unknown value to derive the strain. The same calculation procedures and formulas were applied to both specimens.

Table 4. Formulas for calculation of the crack width.

Base Type	Crack Width	$\varepsilon_{sm} - \varepsilon_{cm}$		Name
EC 2 Part.1–1	$w_k = S_{r.max}(\varepsilon_{sm} - \varepsilon_{cm})$	First [1]	$\frac{f_{so}}{E_s} - \frac{\beta_t f_{ctm}(1+n\rho_e)}{E_s\rho_e}$	E1-1
	$S_{r.max} = 3.4c + 0.425k_1k_2d_b/\rho_e$	Second [2]	$\frac{f_{so}}{E_s}\left(1-(1+n\rho_e)\beta_1\beta_2\left(\frac{f_{scr}}{f_{so}}\right)^2\right)$	E1-2
EC 2 Part.2	$w_k = S_{r.max}(\varepsilon_{sm} - \varepsilon_{cm})$	First [1]	$\frac{f_{so}}{E_s} - \frac{\beta_t f_{ctm}(1+n\rho_e)}{E_s\rho_e}$	E2-1
	$S_{r.max} = d_b/3.6\rho_e$	Second [2]	$\frac{f_{so}}{E_s}\left(1-(1+n\rho_e)\beta_1\beta_2\left(\frac{f_{scr}}{f_{so}}\right)^2\right)$	E2-2
Euro-Design Handbook [3]	$w_k = \beta S_{r.max}\varepsilon_{sm}$	First [1]	$\frac{f_{so}}{E_s}\left(1-\beta_t\frac{f_{scr}}{f_{so}}\right)$	EH-1
	$S_{r.max} = 50 + 0.25k_1k_2d_b/\rho_e$	Second [2]	$\frac{f_{so}}{E_s}\left(1-\beta_1\beta_2\left(\frac{f_{scr}}{f_{so}}\right)^2\right)$	EH-2

[1] $\varepsilon_{sm} - \varepsilon_{cm}$ *or* ε_{sm} is in the form of first-order formula. [2] $\varepsilon_{sm} - \varepsilon_{cm}$ *or* ε_{sm} is in the form of second-order formula. [3] The crack width was calculated by using only ε_{sm} for convenience.

Where, w_k is the crack width, $S_{r.max}$ is the maximum crack spacing, ε_{sm} is the mean strain in the steel reinforcement under the relevant combination of loads, ε_{cm} is the mean strain in the concrete between cracks, c is the cover to the longitudinal reinforcement, k_1 is a coefficient that takes account of the bond properties of the bonded reinforcement (0.8 for high bond bars), β_1 and k_2 are coefficients that takes account of the distribution of strain (0.5 for bending), d_b is the bar diameter, ρ_e is the effective ratio of streel reinforcement, β is the coefficient with relationship between mean crack width and design crack width (1.7 for maximum crack width), f_{so} is the stress in the steel reinforcement assuming a cracked section, n is the ratio E_s/E_c, E_s is elastic modulus of steel reinforcement, E_c is elastic modulus of the concrete, β_t and β_2 are factors dependent on the duration of the load (1.0 for short term loading), f_{ctm} is the mean value of the tensile strength of the concrete ($0.3f_{cm}^{2/3}$), f_{cm} is the mean value of the compressive strength of the concrete ($f_{ck} + 4 \sim 6$ MPa), f_{scr} is the stress in the steel reinforcement when cracked ($ny(M_{cr}/I_{cr})$), y is the $d - x$, d is the effective depth, x is the distance from top of compressive zone to neutral axis, M_{cr} is the cracking moment, and I_{cr} is the cracked moment of inertia [32].

3.2. Estimation Results

The strain of the steel reinforcement, estimated using the crack width for the two specimens, is shown in Figure 7. The formula for crack width consists of components based on when the crack

occurs. Hence, there is a minimum value that exists, which depends on the material properties and coefficient. Therefore, there is an offset of about 1000×10^{-6} mm/mm in the first-order-based formula and about 10×10^{-6} mm/mm in the second-order-based formula in Figure 7. The estimated strain of each specimen was compared with the measured strain at S3, which was closest to the crack that was measured for each specimen. For the integral specimen, the estimated strain was greater than the measured strain at S3 before the yield load was reached. After the yield load was reached, the measured strain increased sharply and was similar to the strain estimated using the first-order formulas (E1-1, E2-1, EH-1). For the modular specimen, the estimated strain was greater than the measured strain and increased sharply after the yield load was reached.

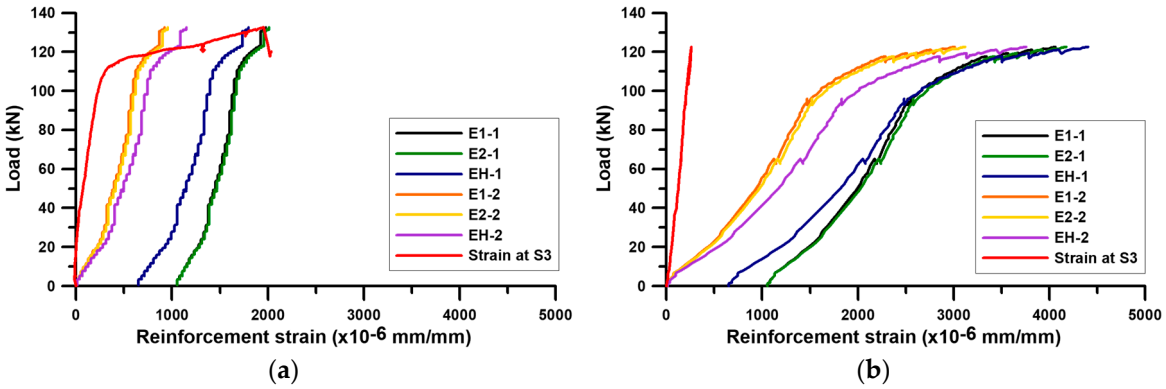

Figure 7. Estimated steel reinforcement strain: (**a**) integral specimen; (**b**) modular specimen.

Tables 5 and 6 present the estimated strains at the yield load and ultimate load. The estimated strain at the yield load was compared with 2000×10^{-6} mm/mm, ε_y, which is the theoretical yield strain of the steel reinforcement, and the estimated strain at the ultimate load was compared with the strain at the yield load.

Table 5. Estimated strains of the integral specimen at the yield and ultimate loads.

Type		Estimated Strain ($\times 10^{-6}$ mm/mm)			
		At Yield Load (ε^*_{yI})	Ratio ($\varepsilon^*_{yI}/\varepsilon_y$)	At Ultimate Load (ε^*_{uI})	Ratio ($\varepsilon^*_{uI}/\varepsilon^*_{yI}$)
First-order formula	E1-1	1676.33	0.838	1974.72	1.178
	E2-1	1699.55	0.850	2009.07	1.182
	EH-1	1426.84	0.713	1799.2	1.261
Average		1600.91	0.800	1927.66	1.204
Second-order formula	E1-2	621.90	0.311	920.2	1.480
	E2-2	645.10	0.323	954.54	1.480
	EH-2	775.95	0.388	1148.25	1.480
Average		680.98	0.340	1007.66	1.480

Table 6. Estimated strains of the modular specimen at the yield and ultimate loads.

Type		Estimated Strain ($\times 10^{-6}$ mm/mm)			
		At Yield Load (ε^*_{yM})	Ratio ($\varepsilon^*_{yM}/\varepsilon_y$)	At Ultimate Load (ε^*_{uM})	Ratio ($\varepsilon^*_{uM}/\varepsilon^*_{yM}$)
First-order formula	E1-1	2720.67	1.360	4063.4	1.494
	E2-1	2782.88	1.391	4175.75	1.501
	EH-1	2730.10	1.365	4405.73	1.614
Average		2744.55	1.372	4214.96	1.536
Second-order formula	E1-2	1666.07	0.833	3008.76	1.806
	E2-2	1728.28	0.864	3121.1	1.806
	EH-2	2079.09	1.040	3754.68	1.806
Average		1824.48	0.912	3294.85	1.806

Regarding the estimated strain at the yield load (Table 5), the average strains estimated using the first- and second-order formulas were 80% and 34%, respectively, of the yield strain (2000×10^{-6} mm/mm). The strains of the ultimate load, estimated using the first- and second-order formulas, were 20.4% and 48% higher, respectively, than the estimated strains of the yield load. At the yield-load stage, the strain estimated using the first-order formula reflected the behavior of the integral specimen, and the second-order formula underestimated the strain compared with the first-order formula.

Regarding the estimated strain at the yield load (Table 6), the average strains, estimated using the first- and second-order formulas, were 137.2% and 91.2%, respectively, of the yield strain (2000×10^{-6} mm/mm) . The strains at the ultimate load, estimated using the first- and second-order formulas, were 53.6% and 80.6% higher, respectively, than the estimated strains at the yield load. The average increment of the estimated strain from the yield load to the ultimate load was 450% that of the integral specimen. At the yield load stage, the strain estimated using the second-order formula reflected the behavior of the modular specimen, and the second-order formula underestimated the strain compared with the first-order formula.

The estimated strains for the integral and modular specimens are compared in Table 7. All the estimated strains of the modular specimen were greater than those of the integral specimen. At the yield loads, the estimates based on the first- and second-order formulas were 71.4% and 167.9% larger, respectively, than those for the integral specimen. At the ultimate loads, the estimates based on the first- and second-order formulas were 118.7% and 227.0% larger, respectively, than those for the integral specimen. These results are attributed to the fact that for the modular specimen, the steel reinforcement of the discontinuity bore a greater load compared with the integral specimen owing to the larger crack width. Therefore, if the same load is applied, the steel reinforcement yield at a discontinuity in the modular specimen would occur earlier than that in the integral specimen.

Table 7. Comparison of the estimated strains for the integral and modular specimens.

Type	Estimated Strain at Yield Load ($\times 10^{-6}$ mm/mm)			Estimated Strain at Ultimate Load ($\times 10^{-6}$ mm/mm)		
	Integral ($\bar{\varepsilon}^{*}_{yI}$)	Modular ($\bar{\varepsilon}^{*}_{yM}$)	Ratio ($\bar{\varepsilon}^{*}_{yM}/\bar{\varepsilon}^{*}_{yI}$)	Integral ($\bar{\varepsilon}^{*}_{uI}$)	Modular ($\bar{\varepsilon}^{*}_{uM}$)	Ratio ($\bar{\varepsilon}^{*}_{uM}/\bar{\varepsilon}^{*}_{uI}$)
Average strain estimated using first-order formula	1600.91	2744.55	1.714	1927.66	4214.96	2.187
Average strain estimated using second-order formula	680.98	1824.48	2.679	1007.66	3294.85	3.270

Table 8 presents the estimated strains at the service, yield, and ultimate loads for comparing the estimated strain changes of the integral and modular specimens. The estimated strains were obtained using the first-order formula for the integral specimen and the second-order formula for the modular specimen, so that the steel reinforcement yielded when the yield load was reached. The service load was applied as 60% of the yield load, which is generally considered to be the serviceability limit state. The average estimated strain of the modular specimen at the service load was 12.9% lower than that of the integral specimen. However, at the yield load stage, the average estimated strain of the modular specimen increased rapidly and was estimated to be 14.0% higher than that of the integral specimen. In the ultimate load stage, the strain gap was widened, and the average estimated strain of the modular specimen was 70.9% higher than that of the integral specimen. Although the second-order formula, which was applied for the modular specimen, underestimated the strain, the estimated strain increased rapidly and exceeded that of the integral specimen at the ultimate load stage. Therefore, as the load increases, the stress and strain concentrated at the discontinuity interface of the joint in the modular specimen increase.

Table 8. Comparison of the estimated strain changes for each load stage.

Base Type	Estimated Strain at Service Load ($\times 10^{-6}$ mm/mm)			Estimated Strain at Yield Load ($\times 10^{-6}$ mm/mm)			Estimated Strain at ultimate load ($\times 10^{-6}$ mm/mm)		
	Integral [1] (ε^*_{sI})	Modular [2] (ε^*_{sM})	Ratio ($\varepsilon^*_{sM}/\varepsilon^*_{sI}$)	Integral [1] (ε^*_{yI})	Modular [2] (ε^*_{yM})	Ratio ($\varepsilon^*_{yM}/\varepsilon^*_{yI}$)	Integral [1] (ε^*_{uI})	Modular [2] (ε^*_{uM})	Ratio ($\varepsilon^*_{uM}/\varepsilon^*_{uI}$)
EC2 part.1-1	1527.14	1143.95	0.749	1676.33	1666.07	0.994	1974.72	3008.76	1.524
EC2 part.2	1544.78	1186.65	0.768	1699.55	1728.28	1.017	2009.07	3121.1	1.554
Euro-Design Handbook	1240.66	1427.49	1.151	1426.84	2079.09	1.457	1799.2	3754.68	2.087
average	1437.53	1252.70	0.871	1600.91	1824.48	1.140	1927.66	3294.85	1.709

[1] Strain was obtained using the first-order formula. [2] Strain was obtained using the second-order formula.

The strain estimated according to Eurocode2 part.1-1 (Table 8) and the strains measured in the experiments (Table 3) are shown in Figure 8 for each load stage: service, yield, and ultimate load. The measured strains at the same location in the service load stage were very similar (Figure 8a), and the estimated strain of the modular specimen was lower than that of the integral specimen (Figure 8b). At the yield load stage, the measured and estimated strains were very similar. However, when the load increased from the yield load to the ultimate load, the strain of the integral specimen, measured at S2 (1000 mm) and S3 (2000 mm), increased by 770.8%, while the strain of the modular specimen increased by only 37.6% at the same locations. In contrast, regarding the estimated strain, the integral specimen exhibited an increase of 17.8%, and that of the modular specimen was 80.6%. Thus, in the modular specimen, only the steel reinforcement at the discontinuity interface of the joint resisted the load, whereas, in the integral specimen, the steel reinforcement uniformly resisted the load in the central section, where a constant moment occurred.

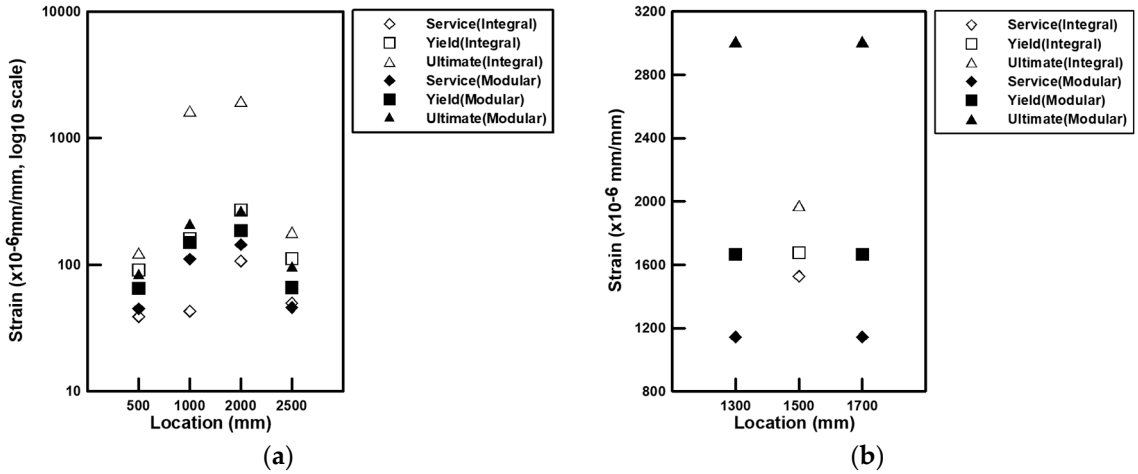

Figure 8. Strain change for each load stage: (**a**) measured strain; (**b**) estimated strain by EC2 Part.1-1.

4. Conclusions

The flexural behavior of a modular specimen with a joint was analyzed quantitatively according to estimation of the steel reinforcement strain and was compared with that of an integral specimen.

1. The load-deflection behavior of the modular and integral specimens was very similar. However, the crack progression and failure patterns differed owing to the joint of the modular specimen. The first crack of the modular specimen occurred at the discontinuity interface, and the maximum crack width was 327% larger than that of the integral specimen.
2. Regarding the steel reinforcement strain measured at the loading point, the strain of the integral specimen increased sharply after the yield load was reached, but that of the modular specimen did not exhibit any change.
3. In the case of the strain estimated according to the crack width, all the estimated strains of the modular specimen were greater than those of the integral specimens, and the gap of the strains

increased with the increasing load. Therefore, if the same load is applied, the steel reinforcement yield at a discontinuity in the modular specimen occurs earlier than that in the integral specimen.

4. At the yield load stage, the strain estimated using the first-order formula reflected the behavior of the integral specimen, and that estimated using the second-order formula reflected the behavior of the modular specimen. Comparing the results obtained using the different formulas revealed that the estimated strain at the service load was lower for the modular specimen than for the integral specimen. However, at the yield and ultimate load stages, the estimated strain of the modular specimen increased rapidly and the strain gap was widened. The measured strain exhibited the opposite result. Therefore, in the modular specimen, only the steel reinforcement at the discontinuity interface of the joint resisted the load, whereas in the integral specimen, the steel reinforcement uniformly resisted the load in the central section, where a constant moment occurred.

It was determined that in the modular specimen, only the steel reinforcement at the discontinuity interface resisted the load. Thus, the steel reinforcement of a modular structure is likely to yield earlier than that of an integral structure. Hence, the safety and quality of the connecting steel reinforcement should be considered in design and construction.

Author Contributions: Writing—original draft and methodology, J.P.; investigation and methodology, H.-K.L.; project administration and supervision, S.-K.P.; methodology, J.C.; writing—review and editing, methodology, S.H.

Funding: This research was supported by a grant from the Construction Technology Innovation Program (10CTIPB01-Modular bridge Research and Business Development Consortium) funded by Ministry of Land, Transportation, and Maritime Affairs (MLTM) of Korea Government.

Conflicts of Interest: The authors declare no conflicts of interest.

References

1. Ehlen, M.A.; Marshall, H.E. *The Economics of New-Technology Materials: A Case Study of FRP Bridge Decking*; National Institute of Standards and Technology: Gaithersburg, MD, USA, 1996.
2. Hawk Hawk, H. *Bridge Life-Cycle Cost Analysis*; Transportation Research Board: Washington, DC, USA, 2002.
3. AASHTO. *Guide Manual for Bridge Element Inspection*, 1st ed.; AASHTO: Washington, DC, USA, 2011.
4. Arduini, M.; Nanni, A. Behavior of Precracked RC Beams Strengthened with Carbon FRP Sheets. *J. Compos. Constr.* **1997**, *1*, 63–70. [CrossRef]
5. Hong, S.; Park, S.K. Effect of Prestress Levels on Flexural and Debonding Behavior of reinforced Concrete Beams Strengthened with Prestressed Carbon Fiber Reinforced Polymer Plates. *J. Compos. Mater.* **2013**, *47*, 2097–2111. [CrossRef]
6. Hong, S.; Park, S.K. Prestressing Effects on the Performance of Concrete Beams with Near-Surface-Mounted Carbon-Fiber-Reinforced Polymer Bars. *Mech. Compos. Mater.* **2016**, *52*, 305–316. [CrossRef]
7. Park, J.; Hong, S.; Park, S.K. Experimental Study on Flexural Behavior of TRM-strengthened RC Beam: Various Types of Textile-Reinforced Mortar with Non-Impregnated Textile. *Appl. Sci.* **2019**, *9*, 381. [CrossRef]
8. Culmo, M.P. *Accelerated Bridge Construction Manual-Experience in Design, Fabrication and Erection of Prefabricated Bridge Elements and Systems*; FHWA-HIF-12-013; Federal Highway Administration: Salem, OR, USA, 2011.
9. Korea Agency for Infrastructure Technology Advancement. *Pohang Iron and Steel Company. Research & Business Development of Modular Bridges*, Final ed.; Korea Agency for Infrastructure Technology Advancement: Anyang, Korea, 2015.
10. Rombach, G.A.; Abendeh, R. Bow-Shaped Segments in Precast Segmental Bridges. *Eng. Struct.* **2008**, *30*, 1711–1719. [CrossRef]
11. Henin, E.; Morcous, G. Non-Proprietary Bar Splice Sleeve for Precast Concrete Construction. *Eng. Struct.* **2015**, *83*, 154–162. [CrossRef]
12. Choi, J.; Park, S.K.; Kim, H.Y.; Hong, S. Behavior of High-Performance Mortar and Concrete Connections in Precast Concrete Elements: Experimental Investigation Under Static and Cyclic Loadings. *Eng. Struct.* **2015**, *100*, 633–644. [CrossRef]

13. Ryu, H.-K.; Kim, Y.-J.; Chang, S.-P. Experimental Study on Static and Fatigue Strength of Loop Joints. *Eng. Struct.* **2007**, *29*, 145–162. [CrossRef]
14. Li, L.; Ma, Z.J.; Griffey, M.E.; Oesterle, R.G. Improved Longitudinal Joint Details in Decked Bulb Tees for Accelerated Bridge Construction: Concept Development. *J. Bridge Eng.* **2010**, *15*, 327–336. [CrossRef]
15. Buyukozturk, O.; Bakhoum, M.M.; Beattie, S.M. Shear Behavior of Joints in Precast Concrete Segmental Bridges. *J. Struct. Eng.* **1990**, *116*, 3380–3401. [CrossRef]
16. Issa, M.I.; Abdalla, H.A. Structural Behavior of Single Key Joints in Precast Concrete Segmental Bridges. *J. Bridge Eng.* **2007**, *12*, 315–324. [CrossRef]
17. Kim, Y.J.; Chung, C.H.; Kim, J.H. Shear Tests on Female-to-Female Type Joint Between Precast Concrete Bridge Decks. *J. Korea Concr. Inst.* **1998**, *10*, 161–168.
18. Lee, J.-M.; Lee, S.-Y.; Song, J.-J.; Park, K.-H. Static Load Tests on Flexural Strength and Crack Serviceability of a Longitudinal Joint for the Slab-Type Precast Modular Bridges. *J. Korea Concr. Inst.* **2015**, *27*, 137–145. [CrossRef]
19. Shah, B.N.; Sennah, K.; Kianoush, M.R.; Tu, S.; Clifford, L. Experimental Study on Prefabricated Concrete Bridge Girder-to-Girder Intermittent Bolted Connections System. *J. Bridge Eng.* **2007**, *12*, 570–584. [CrossRef]
20. Zhu, P.; Ma, Z.J.; Cao, Q.; French, C.E. Fatigue Evaluation of Longitudinal U-Bar Joint Details for Accelerated Bridge Construction. *J. Bridge Eng.* **2012**, *17*, 191–200. [CrossRef]
21. Park, J.; Choi, J.; Lee, H.; Park, S.K.; Hong, S. A Study on the Design of the Top Flange of a Modular T-girder Bridge using the Limit State Design Method. *Appl. Sci.* **2016**, *6*, 381. [CrossRef]
22. Park, J.; Choi, J.; Lee, H.; Park, S.; Hong, S. Evaluation of Structural Behavior and Moment of Inertia on Modular Slabs Subjected to Cyclic Loading. *J. Korea Inst. Struct. Maint. Insp.* **2015**, *19*, 95–102.
23. Park, J.; Choi, J.; Jang, Y.; Park, S.K.; Hong, S. An Experimental and Analytical Study on the Deflection Behavior of Precast Concrete Beams with Joints. *Appl. Sci.* **2017**, *7*, 1198. [CrossRef]
24. Park, J.; Hong, S.; Park, S.K.; Choi, J. A Study on Parameter of Steel Strain of Precast Reinforced Concrete with Joint. In Proceedings of the IABSE Conference, Vancouver 2017: Engineering the Future-Report, Vancouver, BC, Canada, 19–23 September 2017.
25. Lee, H. Comparative Study on the ReBar Strain of RC Flexural Beams with Connection Part. Master's Thesis, Sungkyunkwan University, Seoul, Korea, December 2014.
26. Park, J.; Lee, H.; Choi, J.; Park, S.-K.; Hong, S. Estimate the Steel Strain by Using the Crack of Intersection in the Modular Bridge. In Proceedings of the 23nd International Conference on Composites/Nano-Engineering, Chengdu, China, 12–18 July 2015.
27. European Committee for Standardization. *Eurocode 2: Design of Concrete Structures-Part 1-1: General Rules and Rules for Buildings*; European Committee for Standardization: Brussels, Belgium, 2007; pp. 126–128.
28. European Committee for Standardization. *Eurocode 2: Design of Concrete Structures-Part2: Concrete Bridges (Draft 1.2)*; European Committee for Standardization: Brussels, Belgium, 2002; pp. 148–151.
29. FIB. *Structural Concrete-Manual Textbook*; International Federation for Structural Concrete: Lausanne, Switzerland, 1999; Volume 1.
30. Eibl, J. *Concrete Structures Euro-Design Handbook*; Ernst & Sohn: Berlin, Germany, 1994.
31. CEB-FIP. *CEB-FIP Model Code 90*; Final Draft; CEB-FIP: Lausanne, Switzerland, 1991.
32. Korea Concrete Institute. *Concrete Structures Design Code*, 1st ed.; Korea Concrete Institute: Seoul, Korea, 2012.